Nanoelectromechanical Chip (NELMEC) Combination of Nanoelectronics and Microfluidics to Diagnose Epithelial and Mesenchymal Circulating Tumor Cells from Leukocytes

Seied Ali Hosseini, Mohammad Abdolahad, Somayeh Zanganeh, Mahyar Dahmardeh, Milad Gharooni, Hamed Abiri, Alireza Alikhani, Shams Mohajerzadeh, and Omid Mashinchian*

An integrated nano-electromechanical chip (NELMEC) has been developed for the label-free distinguishing of both epithelial and mesenchymal circulating tumor cells (ECTCs and MCTCs, respectively) from white blood cells (WBCs). This nanoelectronic microfluidic chip fabricated by silicon micromachining can trap large single cells (>12 μm) at the opening of the analysis microchannel arrays. The nature of the captured cells is detected using silicon nanograss (SiNG) electrodes patterned at the entrance of the channels. There is an observable difference between the membrane capacitance of the ECTCs and MCTCs and that of WBCs (measured using SiNG electrodes), which is the key indication for our diagnosis. The NELMEC chip not only solves the problem of the size overlap between CTCs and WBCs but also detects MCTCs without the need for any markers or tagging processes, which has been an important problem in previously reported CTC detection systems. The great conductivity of the gold-coated SiNG nanocontacts as well as their safe penetration into the membrane of captured cells, facilitate a precise and direct signal extraction to distinguish the type of captured cell. The results achieved from epithelial (MCF-7) and mesenchymal (MDA-MB231) breast cancer cells circulated in unprocessed blood suggest the significant applications for these diagnostic abilities of NELMEC.

S. A. Hosseini, Dr. M. Abdolahad, S. Zanganeh, M. Dahmardeh, M. Gharooni, H. Abiri, A. Alikhani, Prof. S. Mohajerzadeh
Nano Electronic Center of Excellence
Nano Bio Electronic Devices Lab and Thin Film and NanoElectronics Lab
School of Electrical and Computer Engineering
University of Tehran
14395/515 Tehran, Iran
E-mail: m.abdolahad@ut.ac.ir

O. Mashinchian
Institute of Bioengineering
School of Life Sciences
Ecole Polytechnique Fédérale de Lausanne (EPFL)
CH-1015 Lausanne, Switzerland

DOI: 10.1002/smll.201502808

1. Introduction

Tumor metastasis is the series of several sequential steps that lead to spread of the cancer in the body and starts by intravasation of individual cells, named circulating tumor cells (CTCs),[1] into the bloodstream. Having originated from the primary tumor, CTCs enumeration procedures are known as reliable methods in cancer staging and therapy monitoring (such as minimal residual disease (MRD)).[2–5] The number of CTCs has a good correlation with various clinical time points such as overall survival (OS) and progression free survival (PFS).[6,7] Less than 5 CTCs could be found per mL of blood sample in cancer patients with high survival rates.[8] Against the billions of red blood cells (RBCs) and millions of WBCs in a typical blood sample detection of such rare

cells is hard.[9] Hence, CTC tracking often requires complicated blood enrichment steps. Due to their heterogeneous binding affinity to the markers and some of their properties being similar to peripheral blood cells, various methods have been investigated for CTC detection.[10,11] The most famous and only FDA (Food and Drug Administration of United States)-approved system so far is CellSearch.[9,12] This system enriches CTCs by means of an epithelial cell-adhesion molecule protein (Ep-CAM) and depends on an immunemagnetic enrichment method. However, the Ep-CAM expression in CTCs is easily lost because of dynamic epithelial-mesenchymal transitions (EMTs).[13]

To overcome the deficiencies of the Ep-CAM based systems the physical properties of CTCs have been investigated and compared to normal blood cells. Some reports have claimed that on average RBCs and WBCs are smaller in size than CTCs.[10] ISET (isolation by size of epithelial tumor cells) is the most famous size-based CTC detection system where a polymeric membrane (with a pore size of 8 μm and fabricated by a particle track etching method) is applied to isolate the CTCs.[14] The size overlap between WBCs and CTCs strongly limits the efficiency of ISET. About 4% of WBCs (such as monocytes and eosinophils) are about 12–20 μm in diameter, which is comparable to the size of CTCs (12 to 35 μm, depending on the type of cancer).[15] So, at least 40 000 WBCs with a similar size to that of CTCs exist in each mL of blood. Size-dependent methods are more suited to CTC clusters in enriched blood samples as used in a new type of microfluidic chips named "cluster chip".[16]

Another suggested method to solve the EMT problem is using complicated markers such as N-Cadherin and Vimentin.[17] Although these markers bind to mesenchymal CTCs (MCTCs), they also suffer from non-desired specific binding to normal blood cells and thus cause positive false responses.[18] MCTCs are more capable of migrating to and invading other tissues.[19,20] Hence, their subsequent detection and characterization steps are of the utmost importance to increase the sustainability of an assay. It seems that further parameters of the cells (such as their electrical properties) must be investigated to distinguish ECTCs and MCTCs from WBCs.

Electrical detection of cancer cells has been investigated by many groups.[21–23] The main idea of this method is to extract a signal from the flowing cells to distinguish cancerous types based on their different dielectric properties from normal cells. Dielectrophoresis,[24,25] as the most famous electrical method, can be used to diagnose the electrical charges of the CTCs and differentiate them from peripheral blood. However, because of its poor efficiency, additional enrichment steps, such as applying hydromechanical[26] forces, are unavoidable. Here, we introduce a nanoelectrically activated microfluidic chip with the ability of distinguishing both ECTCs and MCTCs from large WBCs in unprocessed blood, named nanoelectromechanical CTC chip (NELMEC chip). CTCs and large WBCs (>12 μm) are entrapped at the entrance of vertically etched silicon microchannels. Both types of CTCs could be distinguished from WBCs based on their different membrane capacitance, which was directly measured by conductive Si nanograss electrodes patterned at the opening of the channels. The presence of Si nanograsses enhanced the quality of signal extraction from the entrapped cells without inducing any damage nor membrane rupture to the cells as previously reported by our group.[27]

2. Results and Discussion

2.1. Characterization and Operational Mechanism of the NELMEC Chip

The schematic of the NELMEC chip is presented in **Figure 1**A. The chip was fabricated by a combination of photolithography, micromachining, and nanograss processing (Figure 1B) as described in the Experimental Section. The depth and width of the vertically etched channels were about 15 and 12 μm, respectively (Figure 1B-2). Si nanograss electrodes were produced near the channels by reactive ion etching (RIE) (SensIran Co.) for direct signal extraction from the entrapped cells at the opening of the microchannels (Figure 1C and C-1). Finally, a polydimethylsiloxane (PDMS) layer was prepared and bound on top of the chip to make the completed device. Figure 1D shows electron microscopy images of the NELMEC chip after delivering a blood sample that contained breast CTCs through the channels. The top-side PDMS capping surface, as well as the gold-covered readout pads connected to the signal extraction board, are indicated in the SEM image in Figure 1D-1. By combining size-based capturing with electrical recognizing in one module a synergy of trapping, staging, and detecting on a single chip was achieved. The channels were optimized to let RBCs, small WBCs (<12 μm), and platelets pass through the channels to the waste outlet without a need for further washing.

The array of analysis channels and the SiNG electrodes at the opening of each cavity are clearly observable in Figure 1D-2. The CTCs in our experiments were MCF7 and MDA-MB231 cell lines, the epithelial and mesenchymal types of breast cancer (size: 15–35 μm), respectively, obtained from standard cell banks of the national cell bank of Iran (NCBI). The cells were cultured and stained using acridine orange (A/O) in their vital state to enable us to detect their fluorescent images after any probable entrapment. The cells were then counted and suspended in a dextrose–sucrose (DS), non-conductive media solution. After that, 0.5 mL of the blood sample was prepared as a carrier solution containing 6.1 k μL^{-1} WBCs, which included 48.2% neutrophils, 4.2% eosiniphils, no basophils, 43.1% lymphocytes, and 4.5% monocytes, as counted using an Auto Analyzer (Sysmex KX21). For calibration purposes and to ensure the precise measurements of the electrical data on the nature of the captured cells, the blood cells were stained using Cyto Red (C/R) so that they could be easily distinguished from the CTCs during entrapment. Finally, the blood and cancerous cells were mixed and diluted in 50 cc of DS. The final solution was divided into 10 individual samples (with a volume of 5 mL to prevent possible clogging). Each sample was then introduced into a syringe pump and delivered to the NELMEC chip at a flow rate of 80 $\mu L\ min^{-1}$ (selected from

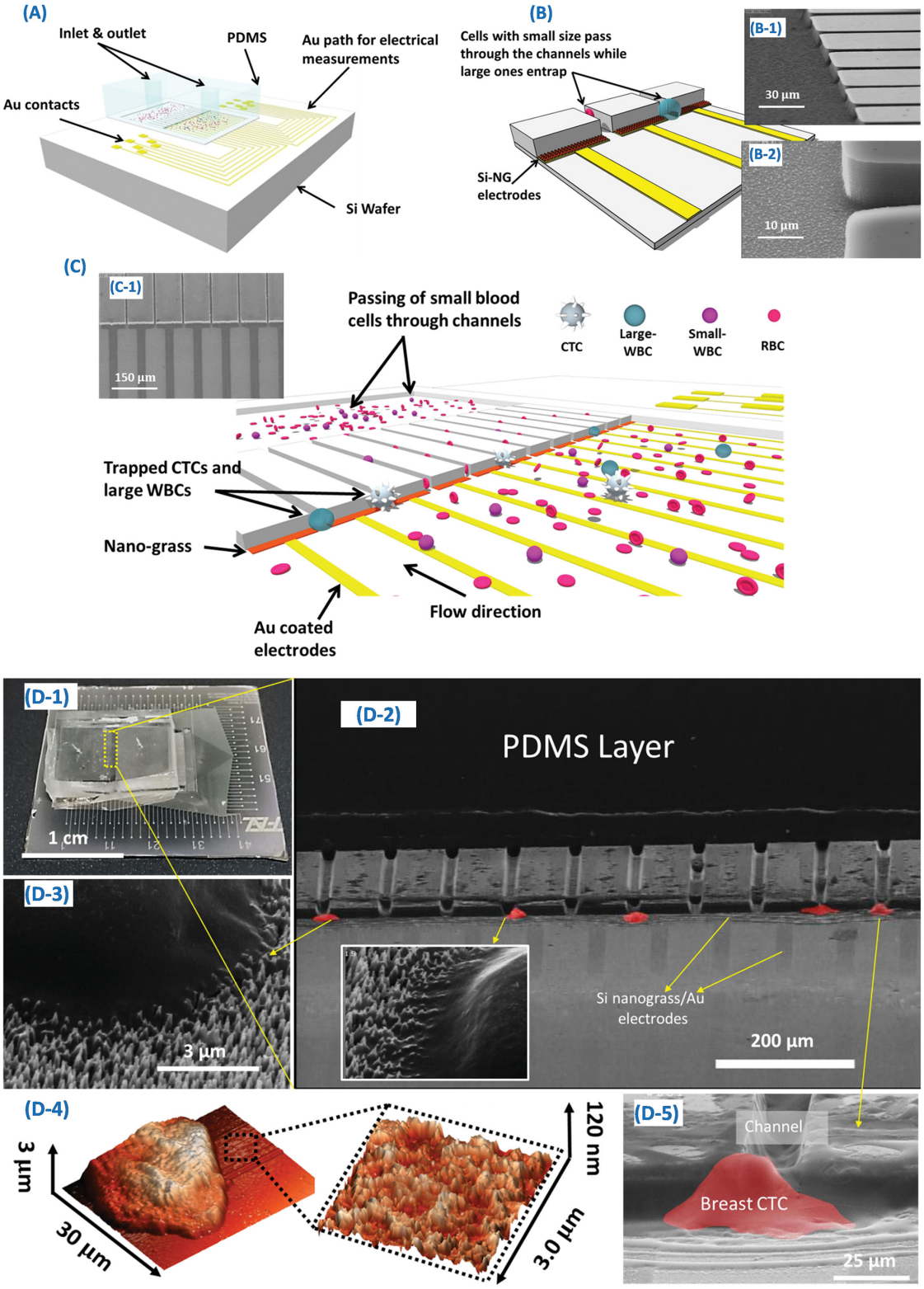

Figure 1. Nanoelectromechanical approach for capturing CTCs. A,B) Schematic of the NELMEC chip, including the channels fabricated by micromachining on the Si surfaces and SiNG electrodes formed at the bottom of their opening. The insets show zoomed-in SEM images of the channels before (B-1) and after (B-2) removing the Cr mask. C) Schematic of the NELMEC chip exposed to unprocessed blood. RBCs and small WBCs passed through the channels whereas CTCs and large WBCs were captured on the nanograss electrodes at the entrance of the trenches. C-1) SEM images of the formed channels and patterned nanoelectrodes. D) SEM images of entrapped CTCs in the NELMEC chip. Panel (D-3) and the inserted image in panel D-2 present the direct interaction between the SiNG nanocontacts and the membrane of the captured cells. Panel D-4 shows the AFM topography of the cells attached to the electrodes.

various flow rates ranging from 20 to 160 μL min^{-1}). Electrical measurements were performed before, during, and after flowing of the solution through the chip. Real-time monitoring of the channels was performed by applying a bias voltage of 40 mV on each couple of electrodes and measuring the impedance at frequencies ranging from 10 kHz to 50 kHz to ensure the recording of any cellular capturing interactions with the SiNG electrodes.

Responses from cell membranes to this type of stimulating signals have been reported to be in this range of frequencies,[23,27,28] as the current-blocking behavior of the membrane for any trapped cell is significant due to beta-dispersion phenomena.[27]

2.2. Capability of NELMEC to Distinguish ECTCs and MCTCs from Leukocytes

Real-time direct electrical signal extraction from the membrane by SiNG/Au nanoelectrodes would be the best solution to distinguish the nature of entrapped cells based on the different intrinsic electrical properties of cancerous cells and leukocytes.[29] Nanograss-incorporated silicon electrodes form a suitable sensing media as they provide many electrically active adhesive sites for the cell membrane (Figure 1D-2 (in-situ) and D-3). Atomic force microscopy (AFM) topographies taken from the entrapped cells and SiNG electrodes (Figure 1D-4) present the direct attachment of the cells on top of the nanograsses with a rms roughness of about 80 nm. Here, the great conductivity of such nano-contacts improved the signal extraction through the membrane of the captured cells (Figure 1D-5) without inducing any perturbation in their vitality (Supporting Information, Figure S1). As a result, any slight variations in current flow caused by the cell membrane through beta dispersion phenomena could be precisely sensed. Finally, the response was a great reflection of the membrane's dielectric properties.

To eliminate the effect of the medium and the intrinsic impedance of the channels, the differentiated impedance value were calculated before, during, and after passing of the solution through the channels. **Figure 2**A and B present the mean changes in the impedance of the SiNG electrodes when a whole blood sample was delivered to the NELMEC chip. The plot was extracted from the scanned impedance diagrams of each channel in individual devices containing a blood sample mixed with ECTCs (Figure 2A: MCF-7) and MCTCs (Figure 2B: MDA-MB-231) at frequencies in the range of 10–50 kHz. The impedance of the channels closed by entrapped ECTCs (Figure 2C: A/O stained green cells) showed 1.3-5 times higher variations than that of channels closed by trapped WBCs (Figure 2D: C/R stained red cells). As shown in Figure 2A, which shows the responses from different channels, the responses of Ch99 vs. Ch56 and Ch42 vs. Ch38 indicate the minimum and maximum impedance variations between WBC- and ECTC-trapped channels, respectively (45% vs. 25% and 77% vs. 16%, respectively). Our results have been confirmed before by known bioelectrical evidence. Tumor cells have been shown to have a higher unit membrane capacitance and lower cytoplasm conductance compared to leukocytes.[29] Hence, their entrapment induces more considerable variations in the impedance of the SiNG electrodes. The measured impedance changes of the channels enclosed by MCTCs (Figure 2E: A/O stained green cells) was a little sharper than that of ECTCs. The impedance changes in the microchannels entrapping the MCTCs (Figure 2B), were 1.8–6 times higher than those of channels entrapping WBCs (Ch69 vs. Ch67 and Ch47 vs. Ch20, respectively). This data completely supports the increasing effect of EMT on the membrane capacitance of tumor cells.[29,30] The responses of the NELMEC chip to the sample solution reveal that this new architecture provides a reliable label-free CTC detection assay using an electromechanical procedure.

2.3. Identifying the Response Range of Captured CTCs and WBCs

The entrapped WBCs might be any of a range of different leukocytes. However, our investigation revealed that the differences between the different leukocytes did not interfere with the response and efficiency of the NELMEC for diagnostic purposes. The highest and lowest capacitances of entrapped WBCs, measured for lymphocytes and neutrophils, induced 25% and 15% deviations, respectively, in the impedance of any microchannel (**Figure 3**A). The range of impedance variations caused by entrapped WBCs is thus smaller than that of CTCs.

On the other hand, the impedance changes in the channels closed by different MCF-7 and MDA-MB231 cells showed deviations from 42 to 75% and 45 to 85%, respectively (red columns in Figure 2A,B, respectively). This might be related to the shape, size, and state (from G_0 to M_2) of the cancer cells during entrapment. Dissimilar geometries of entrapped MCF-7 cells were investigated by confocal microscopy (Figure 3B). The shape and spindle of microtubules (MTs) stained with FITC conjugated with alpha antitubulin, showed the different outward parameters of the entrapped CTCs, which may affect the electrical response of the cells. It is well known that mechanical aspiration on MTs (such as entrapping aspiration by the microchannels of the NELMEC chip) could affect the functional parameters of the membrane.[31,32] Moreover, flow cytometry taken from the CTC samples indicated that the cells were distributed between the G_0 and M_2 states. The coefficient of variation (CV) of the G_0G_1 peak of the MCF-7 cells was 4.3 and the cell-cycle phase fractions of G_0G_1, S, and G_2M were 47.9, 21.9, and 30.2%, respectively (Figure 3C). The same fractions were calculated for MCTCs (Figure 3C-2) and we found that they were 59.8, 15.5, and 33.7%, respectively (Figure 3D). The various vital states and MT configurations of the CTCs might lead to their different electrical responses after entrapment. However, such distributed responses did not show any overlapping with entrapped blood cells.

Monitoring the time evolution of the electrical responses of the electrodes, during the flowing of the solution, could help in elaborating the detecting mechanism of the NELMEC chip. Figure 3E presents the impedance-frequency spectrum for 4 different channels (no cell, WBC, ECTC, and MCTC trapped channels as plotted in Figure 3E-1, E-2, E-3, and E-4 respectively) at three time intervals: namely before flowing

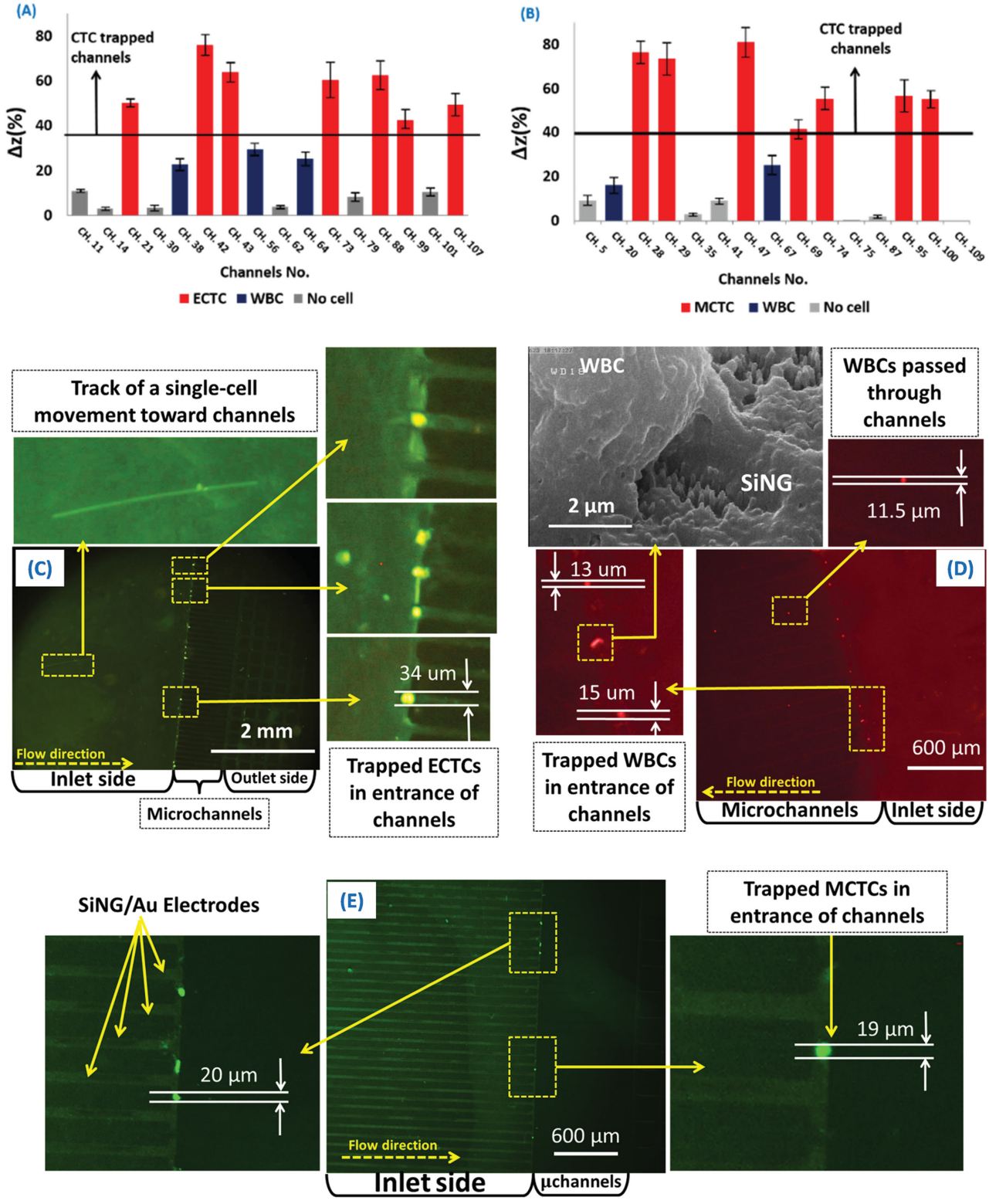

Figure 2. Capture and diagnosis of ECTCs, MCTCs, and large WBCs. A,B) CTCs spiked after being captured by the channels of the NELMEC chip with single-cell resolution. The intensity of the electrical spikes measured by the SiNG electrodes was completely distinguishable between entrapped CTCs and WBCs. The error bars represent the standard error of the mean (number of measurements on each channel = 4). C–E) Representative fluorescence images of entrapped MCF-7 (C), WBC (D), and MDA-MB231 (E) cells, which support the electrical responses of the NELMEC. An SEM image of an entrapped WBC is displayed in the inset of panel D. As is visible in all panels, only cells larger than 12 µm were captured by the microfluidic channels. Here, non-targeted cells (small leukocytes) were delivered to the outlet. It can be seen that a WBC with a diameter of 11.5 µm was not entrapped and left the channel (top inset image in (D).

www.MaterialsViews.com

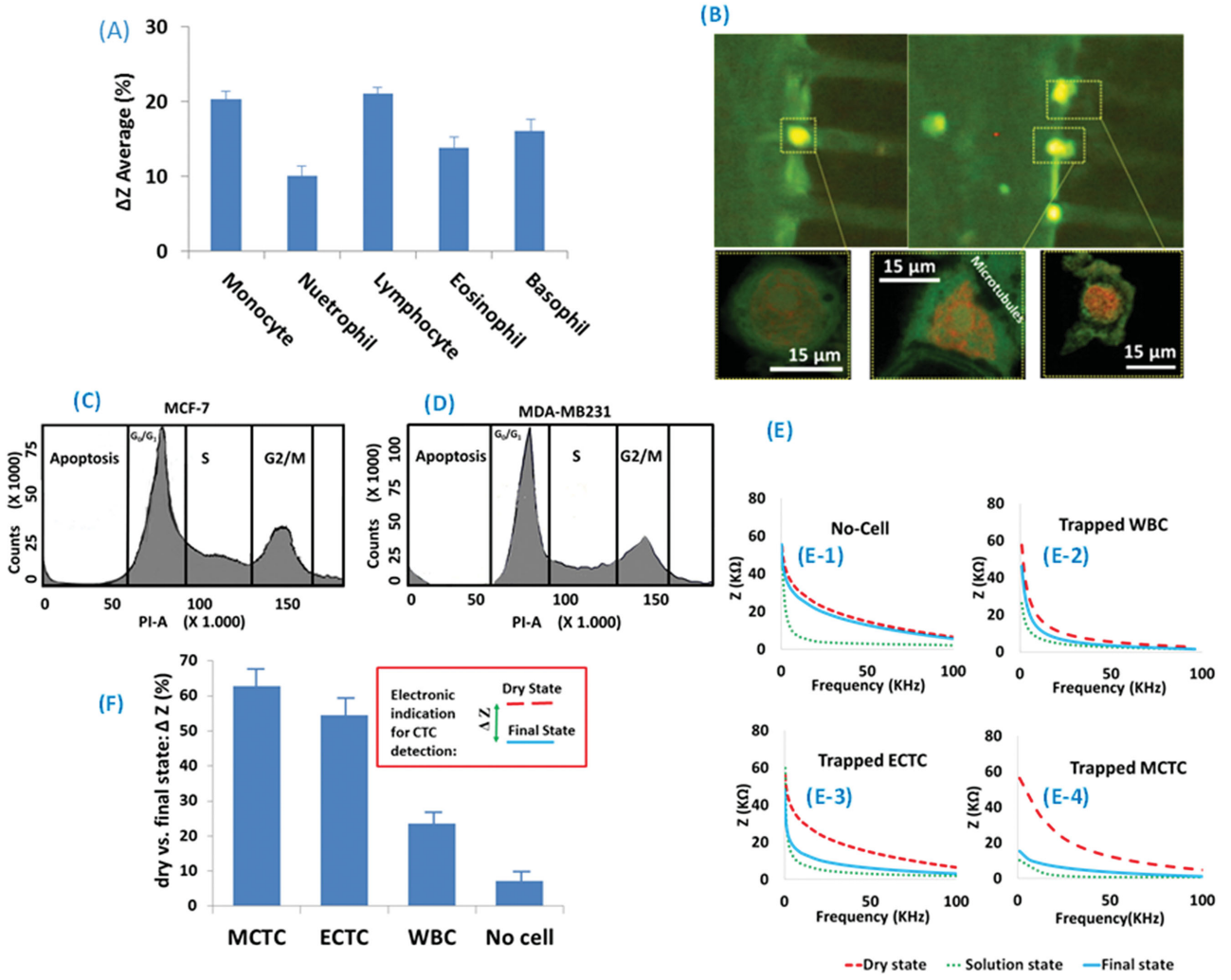

Figure 3. Effect of cellular type, vital state, and shape during the entrapment on the electrical spikes in the NELMEC. A) Impedance variations induced by different types of WBCs. A standard error of the mean was extracted from 5 measurements. B) Confocal images presenting the shape and microtubules' configurations of individual entrapped CTCs. C,D) Flow cytometry analysis of MCF-7 (C) and MDA-MB231 (D) cells showing distributed stages between growth and mitosis for all of them, which desirably affected the electrical response of the entrapped cells. E) The electrical spike of each channel was derived from the response in dry, solution, and final states as represented by a sample channel that remained open (E-1) or enclosed by WBC (E-2), ECTC (E-3), and MCTC (E-4). F) Apart from the spike profile, we also achieved mean impedance variations for each type of entrapped cells as a diagnostic indication of the NELMEC chip. The error bars represent the standard error of the mean (number of measured channels = 15).

the solution into the chip (dry state), while the solution was passing through the channels (solution state), and after all of the solution had left the microchip (final state). The highest impedance value was measured for all of the channels in the dry state. During the solution state, the impedances of both the open and closed channels (by entrapped cells) were induced by the carrier medium solution. During the solution state entrapment of cells at the opening of the channels may have occurred but the presence of the highly resistive DS media probably interfered with the electrical response of the electrodes and thus suppressed the significant electrical spikes in the enclosed channels. So, the solution state might not be best suited for detecting the nature of the entrapped cells. In the final state, the channels that had remained open presented a high impedance similar to that of the dry state (solid curve in Figure 3E-1). But because of the cell-membrane capacitance, the impedance of the channels that had been closed by CTCs or WBCs was observably reduced with respect to that of their dry state. Hence, the impedance differences between the dry and final states in each channel is indicative for the nature of the entrapped cell. The average of the impedance differences that depend on the nature of the entrapped cells have been plotted for all open and closed channels (Figure 3F). These results reveal that CTC entrapment induces a considerable change in the electrical response of the channels.

2.4. Capture Yield and Performance of NELMEC

After having confirmed the distinguishing capability of the NELMEC between WBCs and different types of CTCs, we

attempted to optimize the performance of our chip by flowing MCF-7 and MDA-MB231 cells through the microchannels under various conditions. Firstly, the desired flow rate was determined by examining the capture efficiency of 100 cancer cells that are flowed through the device at various velocities. The results (**Figure 4**A) suggested that around 80 μL min^{-1} appeared to be the optimal flow rate to achieve the highest capture efficiency (as high as 98%). Different ratios of WBCs vs. RBCs (100: around 7×10^4 and 1000: around 7×10^5 in 2 mL DS) were then loaded under the selected flow rate to evaluate the capture efficiency of large WBCs (as stated above, less than 5% of WBCs are in the size range of CTCs). As indicated in Figure 4B (solid columns), about 5% of WBCs were captured by the microchannels. So, the capture efficiencies of the NELMEC for large WBCs was higher than 95%. Interestingly, the captured cells at the entrance of the Si microchannels could be released by reverse pumping with a release efficiency of about 86% (Figure 4B, patterned columns). Moreover, by simply washing with cell lysis solution (NP40 Cell Lysis Buffer) followed by phosphate-buffered saline (PBS), the rest of the remaining cells could be removed from the chip. Finally, the performance of NELMEC was investigated in artificially spiked blood samples by mixing pre-counted CTCs (MCF-7 and MDA-MB231 cancer cells) with whole blood samples from healthy volunteers that was diluted in DS solution. Figure 4C shows a great preference of NELMEC for the type of entrapped cancer cells with a capture yield of more than 94%. Also, the release performance of the chip achieved by reverse pumping (Figure 4D) was just 8–10% less than the capture yield.

In clinical applications, it would be possible to use multiplexed arrays of NELMEC chips to extract real-time signals from a 10 mL blood sample to detect the presence of any epithelial or mesenchymal CTCs with label-free and sharp responses.

3. Conclusions

We introduced a new solution based on nanoelectronics, micromachining, and the unique bioelectrical properties of cells to solve both the EMT and size-overlapping problems in CTC detection. The developed electrically activated microfluidic system (named NELMEC) was used to discriminate ECTCs and MCTCs from WBCs in an unprocessed blood sample without the need for any pre-filtering or labeling. Non-specific fouling, which has generally been a concern for such procedures, was completely solved in this system. Here, large blood cells as well as CTCs were entrapped at the opening of silicon micromachined channels. The nature of the trapped cells could be determined by looking at the electrical signal that was directly extracted from the cell membrane using silicon nanograss (SiNG) electrodes patterned at the entrance of the channels. The data was extracted in the form of an impedance magnitude, which let us gain insight into the capacitive and resistive nature of the large WBCs and CTCs. The membrane capacitance of captured ECTCs and MCTCs was observably lower than that of WBCs, which gave a major indication in our diagnosis. Also, the increased membrane capacitance of MCTCs tended to lead to higher spikes

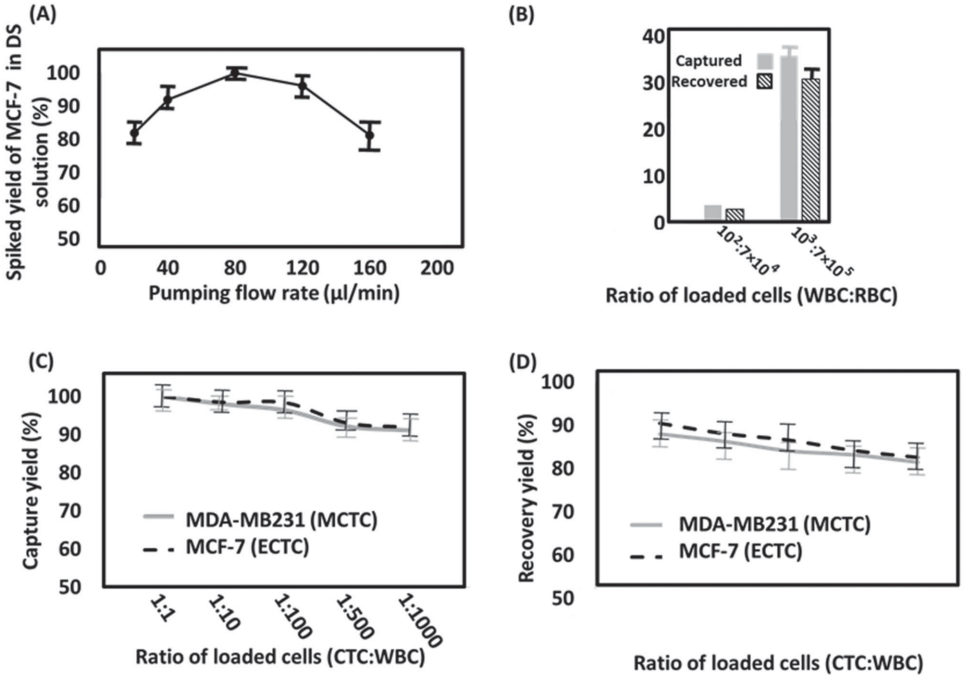

Figure 4. Capture yield of the NELMEC. A) Effect of flow rate on the entrapment of MCF-7 cells suspended in DS solution. The best performance was achieved at a flow rate of 80 μL min^{-1}. B) Capture and recovery yields of WBCs suspended in RBCs at various ratios. About 5% of the WBCs were entrapped. The release yields of the WBCs were about 10% less than the capture yields. C,D) Capture (C) and release yields (D) of MCF-7 (ECTC) and MDA-MB-231 (MCTC) cells in the blood sample. The ratio of the loaded cells ranged from 1 to 0.001. A fixed number of cancer cells and WBCs were mixed with RBCs and DS to achieve the measured values. The error bars represent the standard error of the mean (number of individual tests = (A):4, (B): 3, (C) and (D):4)

in their impedance variation than that of ECTCs. The EMT problem, which is one of the main disadvantages of previously reported CTC detection systems, has been solved in the NELMEC system without the need for additional labeling. The capture yield of the system was between 92 to 97%. This system shows great promise for the enumeration of CTCs in whole blood samples.

4. Experimental Section

Fabrication Process of the NELMEC Chip: The schematic of the fabricated device is presented in Figure 1A,B. A silicon wafer was used as the base of the NELMEC chip. Before use the wafers were thoroughly cleaned using a standard RCA #1 cleaning method ($NH_4OH/H_2O_2/H_2O$ solution at a volume ratio of 1:1:5). Subsequently, a thin layer (ca. 300 nm) of Cr was grown on the substrate by electron-beam coating (Veeco Co.) as a hard mask for silicon vertical etching. Next, the Cr layer was patterned by photolithography to form the shape of the microfluidic channels and the solution reservoir. The chip was then put in a reactive ion etching (RIE) (SensIran Co.) system so all of the non-chromium regions were etched away assisted by SF_6, H_2, and O_2 gases using a 13.6 MHz electromagnetic wave. The details of the etching procedure have been discussed elsewhere.[33] The depth and width of the vertically etched channels were about 15 and 12 μm, respectively. Subsequently, the remaining Cr layer was chemically removed and a thin layer of SiO_2 (300 nm) was grown on the whole of the surface using a wet oxidation furnace (Figure 1B-2). In the next step the oxide layer was patterned followed by producing SiNG electrodes in the desired region (defined by photolithography) by RIE, as described elsewhere.[34] Next, a thin layer of gold (20 nm) coating was patterned by a sputtering system (Veeco Co.) to form the conductive connections and read-out pads. Finally, a passivation layer of Si_3N_4 was deposited by RF-sputtering to cover the region between the SiNG electrodes and the read-out pads as final passivation layer (Figure 1C-1). Finally, a polydimethylsulfoxide (PDMS) layer (Sylgard 184 and curing agent, Sigma-Aldrich Co.) was prepared and bonded on top of the chip by plasma treatment to make the completed microfluidic system presented in Figure 1C-1.

The top-side PDMS capping surface, as well as the gold-covered readout pads, connected to the signal-extraction board, is indicated in the images. Also, arrays of analysis channels and SiNG-electrodes at the opening of each cavity connected to the read-out pad can be observed (Figure 1C-2).

Preparation of Blood Samples: MCF7 and MDA-MB231 cell lines, which are the epithelial and mesenchymal types of breast cancer, respectively, were obtained from standard cell banks of the National Cell Bank of Iran (NCBI). The cells were kept at 37 °C (5% CO_2, 95% air) in Roswell Park Memorial Institute (RPMI)-1640 medium (Sigma 8758) supplemented with 5% fetal bovine serum (Gibco), and 1% penicillin/streptomycin (Gibco). The medium was replaced every other day. Cells were stably stained with A/O in their live state to enable the capturing of fluorescent images of the trapped cells after every experiment. The cells were counted and suspended in 50 mL of dextrose-sucrose (DS) added to 0.5 mL of unprocessed blood as carrier solution containing 6.1 k μL^{-1} WBCs. The distribution of leukocytes was as follows: 48.2% neutrophils, 4.2% eosinophils, no basophils, 43.1% lymphocytes, and 4.5% monocytes, which was monitored by an Auto Analyzer (Sysmex KX21). The blood cells were stained with Cyto Red before dilution.

Blood Testing Procedure by NELMEC: 0.5 mL of blood was diluted in 50 mL of DS to reduce the conductivity of the solution (DS dielectric constant: 80). 10 Individual samples with a volume of 5 mL each were prepared. Known numbers of MCF-7 (ECTC) and MDA-MB 231 (MCTC) cells were added to each sample. Then they were introduced into a syringe pump and delivered to the individual NELMEC chips at a flow rate of 80 $\mu L\ min^{-1}$.

To calibrate the system and show the efficiency and performance of the NELMEC we needed to count the WBCs to have a known ratio of mixed CTCs with WBCs. We used HetaSep to remove the RBCs from the blood sample. HetaSep is an erythrocyte aggregation agent used to quickly separate nucleated cells from RBCs. Its effectiveness is based on the principle that aggregated erythrocytes settle much faster than dispersed cells. We added 150 μL of Dulbecco's phosphate buffered saline (D-PBS) with 2% fetal bovine serum (FBS) (Catalog #07905) and 40 μL HetaSep to 50 μL of fresh blood sample. The mixing needed to be done without producing any bubbles (with a pipette). Then, we incubated the sample for 15–20 min in a 37 °C incubator. This step was best done by placing tubes in a culture incubator as opposed to a water bath, to avoid introducing any probable contamination by residual water when the tube was opened. Subsequently, the upper phase was removed using a micropipette and transferred to a new tube. We slowly aspirated the upper phase, while moving the tip downward without disturbing the RBC pellet.

Electrical Measuring Procedure of NELMEC: The electrical responses of the entrapped cells were carried out using a NI DAQ USB 6323 connected to the sensors by coaxial wires. We designed and fabricated a read-out electronic board with a signal-extracting mechanism (IC No. AD5933). Measurements were performed under an applied voltage of 40 mV on each couple of SiNG electrodes. The real-time monitoring of the channels was performed by measuring the impedance at frequencies ranging from 10 kHz to 50 kHz. Signal extraction was started by introducing the solution into the channels. The signaling was repeated after the solution was gone from the NELMEC chip to detect any cellular capturing interactions with the SiNG electrodes. The final electrical spikes in each channel were the mean value of subsequent measurements indicated in Figure 2 and 3 by error bars. To eliminate the effect of the medium, the difference in impedance values was calculated by comparing the response of the electrodes at various stages of solution flowing.

Fluorescent Imaging from the Entrapped Cells: To investigate the accuracy of the electrical results, CTCs and WBCs were stained with A/O (green) and Cyto Red (Red), respectively, before flowing into the microfluidic chip. Live fluorescent imaging was carried out on the individual cells as per the manufacturer's instructions and the cells were kept in an incubator for 20 min. Then the cells were mixed with DS and flowed by a syringe pump into the NELMEC chip. Phase-contrast images of the cells were taken after their entrapment at the entrance of the microchannels using a JENUS fluorescent microscope with a CCD camera in the monochromatic phase-contrast mode.

Characterization of the Microtubules Distribution of the CTCs by Confocal Microscopy: The effects of cell aspiration and entrapment on the microtubules distribution of the captured CTCs were assessed by inverted confocal microscopy (Leica, TCS SP5, Germany). Prior to imaging, the cells were fixed using a 4% formaldehyde solution for 15 min and permeabilized for 10 min at room temperature with 1% Triton X-100 dissolved in PBS. Cells were diluted in PBS and stained with Anti-alpha tubulin-FITC conjugate (Green) (Sigma-Aldrich) and incubated for 30–45 min. The cell nuclei were stained with propidium iodide (PI) (Invitrogen, USA). Leica Application Suite Advanced Fluorescence (LAS AF) software (Leica Microsystems) was utilized to analyze the confocal microscope pictures.

Supporting Information

Supporting Information is available from the Wiley Online Library or from the author.

Acknowledgements

S.A.H., M.A., S.Z., M.G., and H.A. contributed equally to this work. M. Abdolahad thanks the Iran National Science Foundation (INSF) for their support in this investigation.

[1] S. Mocellin, U. Keilholz, C. R. Rossi, D. Nitti, *Trends Mol. Med.* **2006**, *12*, 130.
[2] S. C. P. Williams, *Proc. Natl. Acad. Sci. USA* **2013**, *110*, 4861.
[3] J. L. Harris, M. Stocum, L. Roberts, C. Jiang, J. Lin, K. Sprott, *Drug Develop. Res.* **2013**, *74*, 138.
[4] M. Thalgott, B. Rack, T. Maurer, M. Souvatzoglou, M. Eiber, V. Kre, M. M. Heck, U. Andergassen, R. Nawroth, J. E. Gschwend, M. Retz, *J. Cancer Res. Clin.* **2013**, *139*, 755.
[5] S.-J. Dawson, D. W. Y. Tsui, M. Murtaza, H. Biggs, O. M. Rueda, S.-F. Chin, M. J. Dunning, D. Gale, T. Forshew, B. Mahler-Araujo, S. Rajan, S. Humphray, J. Becq, D. Halsall, M. R. C. Path, M. Wallis, D. Bentley, C. Caldas, N. Rosenfeld, *New Engl. J. Med.* **2013**, *368*, 1199.
[6] H. J. Yoon, M. Kozminsky, S. Nagrath, *ACS Nano* **2014**, *8*, 1995.
[7] S. Nagrath, L. V. Sequist, S. Maheswaran, D. Bell, D. Irimia, L. Ulkus, M. R. Smith, E. L. Kwak, S. Digumarthy, A. Muzikansky, *Nature* **2007**, *450*, 1235.
[8] T. Yap, D. Lorente, A. Omlin, D. Olmos, J. de Bono, *Clin. Cancer Res.* **2014**, *20*, 2553.
[9] C. Alix-Panabières, K. Pantel, *Nat. Rev. Cancer* **2014**, *14*, 623.
[10] A. Williams, M. Balic, R. Datar, R. Cote, *Recent Res. Cancer* **2012**, *195*, 87.
[11] S. L. Stott, C.-H. Hsu, D. I. Tsukrov, M. Yu, D. T. Miyamoto, B. A. Waltman, S. M. Rothenberg, A. M. Shah, M. E. Smas, G. K. Korir, *Proc. Natl. Acad. Sci. USA* **2010**, *107*, 18329.
[12] R. Sabine, F. Herbert, M. Volkmar, R. Thomas, S. Christian, R. Brigitte, J. Wolfgang, C. Cornelia, B. Katrin, J. Fritz, *Clin. Cancer Res.* **2007**, *13*, 920.
[13] N. M. Karabacak, P. S. Spuhler, F. Fachin, E. J. Lim, V. Pai, E. Ozkumur, J. M. Martel, N. Kojic, K. Smith, P.-i. Chen, *Nat. Protocols* **2014**, *9*, 694.
[14] G. Vona, A. Sabile, M. Louha, V. Sitruk, S. Romana, *Am. J. Pathol.* **2000**, *156*, 57.
[15] S. Arya, B. Limb, A. Abdur Rahman, *Lab Chip* **2013**, *13*, 1995.
[16] A. F. Sarioglu, N. Aceto, N. Kojic, M. C. Donaldson, M. Zeinali, B. Hamza, A. Engstrom, H. Zhu, T. K. Sundaresan, D. T. Miyamoto, *Nat. Methods* **2015**, *12*, 685.
[17] S. A. Mani, W. Guo, M. J. Liao, E. N. Eaton, A. Ayyanan, A. Y. Zhou, F. Brooks, M. Reingard, C. C. Zhang, M. Shipitsin, *Cell* **2008**, *133*, 704.
[18] N. Bednarz, E. Eltze, A. Semjonow, M. Rink, A. Andreas, L. Mulder, J. Hannemann, M. Fisch, K. Pantel, H. G. Weier, *Clin. Cancer Res.* **2010**, *16*, 3340.
[19] M. Yu, D. T. Ting, S. L. Stott, B. S. Wittner, F. Ozsolak, S. Paul, J. C. Ciciliano, M. E. Smas, D. Winokur, A. J. Gilman, *Nature* **2012**, *487*, 510.
[20] M. Yu, A. Bardia, B. S. Wittner, S. L. Stott, M. E. Smas, D. T. Ting, S. J. Isakoff, J. C. Ciciliano, M. N. Wells, A. M. Shah, *Science* **2013**, *339*, 580.
[21] Y.-K. Chung, J. Reboud, K. C. Lee, H. M. Lim, P. Y. Lim, *Biosens. Bioelectron.* **2011**, *26*, 2520.
[22] M. Abdolahad, M. Taghinejad, H. Taghinejad, M. Janmaleki, S. Mohajerzadeh, *Lab Chip* **2012**, *12*, 1183.
[23] M. Abdolahad, M. Janmaleki, M. Taghinejad, H. Taghnejad, F. Salehi, S. Mohajerzadeh, *Nanoscale* **2013**, *5*, 3421.
[24] D. Miyamoto, L. Sequist, R. Lee, *Nat. Rev. Clin. Oncol.* **2014**, *11*, 401.
[25] F. Fabbri, S. Carloni, W. Zoli, P. Ulivi, G. Gallerani, P. Fici, E. Chiadini, A. Passardi, G. L. Frassineti, A. Ragazzini, *Cancer Lett.* **2013**, *335*, 225.
[26] H. Esmaeilsabzali, T. V. Beischlag, M. E. Coxd, A. M. Parameswaranc, E. J. Parka, *Biotechnol. Adv.* **2013**, *31*, 1063.
[27] M. Abdolahad, H. Shashaani, M. Janmaleki, S. Mohajerzadeh, *Biosens. Bioelectron.* **2014**, *59*, 151.
[28] M. Abdolahad, A. Saeidi, M. Janmaleki, O. Mashinchian, M. Taghinejad, H. Taghinejad, S. Azimi, M. Mahmoudi, S. Mohajerzadeh, *Nanoscale* **2015**, *7*, 1879.
[29] P. R. C. Gascoyne, S. Shim, J. Noshari, F. F. Becker, K. Stemke-Hale, *Electrophoresis* **2013**, *34*, 1042.
[30] D. Schneider, M. Tarantola, A. Janshoff, *BBA-Mol. Cell Res.* **2011**, *1813*, 2099.
[31] S. de Keijzer, J. Galloway, G. S. Harms, P. N. Devreotes, P. A. Iglesias, *BBA-Biomembranes* **2011**, *1808*, 1701.
[32] D. J. Stephens, *J. Cell Sci.* **2012**, *125*, 2795.
[33] A. Sammak, S. Azimi, N. Izadi, B. K. Hosseinieh, S. Mohajerzadeh, *J. Microelectromech. Systems* **2007**, *16*, 912.
[34] M. Mehran, Z. Sanaee, M. Abdolahad, S. Mohajerzadeh, *Mater. Sci. Semiconductor Proc.* **2011**, *14*, 199.

Received: September 17, 2015
Revised: November 28, 2015
Published online: January 5, 2016

